Water-Mediated Reversible Control of Three-State Double-Stranded Titanium(IV) Helicates

Naoki Ousaka,[†,‡,§] Manabu Itakura,[†] Akira Nagasaka,[‡] Masaki Ito,[†] Tomonari Hattori,[‡] Daisuke Taura,[†,‡] Tomoyuki Ikai,[†] and Eiji Yashima*[,†,‡]

[†] Department of Molecular and Macromolecular Chemistry, Graduate School of Engineering, Nagoya University, Chikusa-ku, Nagoya 464-8603, Japan.

[‡] Department of Molecular Design and Engineering, Graduate School of Engineering, Nagoya University, Chikusa-ku, Nagoya 464-8603, Japan.

ABSTRACT: A stimuli-responsible reversible structural transformation is of key importance in biological systems. We now report a unique water-mediated reversible transformation between three discrete double-stranded dinuclear titanium(IV) achiral *meso*- and chiral *racemo* (*rac*)-helicates linked by a mono-μ-oxo or a bis(μ-hydroxo) bridge between the titanium ions through hydration/dehydration or its combination with a water-mediated dynamic cleavage/reformation of the titanium-phenoxide (Ti-OPh) bonds. The bis(μ-hydroxo) bridged titanium(IV) *meso*-helicate prepared from two tetraphenol strands with titanium(IV)oxide was readily dehydrated in CD_3CN containing a small amount of water upon heating accompanied by Ti-OPh bonds cleavage/reformation catalyzed by water, resulting in the formation of the mono-μ-oxo bridged *rac*-helicate, which reverted back to the original bis(μ-hydroxo) bridged *meso*-helicate upon hydration in aqueous CD_3CN. These reversible transformations between the *meso*- and *rac*-helicates were also promoted in the presence of a catalytic amount of an acid, which remarkably accelerated the reactions at lower temperature. Interestingly, in anhydrous CD_3CN, the bis(μ-hydroxo) bridged *meso*-helicate was further slowly converted to a different helicate, while maintaining its *meso*-helicate framework, namely, the mono-μ-oxo bridged *meso*-helicate, through dehydration upon heating and its *meso*-to-*meso* transformation was significantly accelerated in the presence of cryptand [2.2.1], which contributes to removing Na^+ ions coordinated to the helicate. Upon cooling, the backward *meso*-to-*meso* transformation took place via hydration. Hence, three different, discrete double-stranded chiral *racemo*- and achiral *meso*-titanium(IV) helicates linked by a mono-μ-oxo or a bis(μ-hydroxo) bridge were successfully generated in a controllable manner by a change in the water content of the reaction media.

Introduction

The metal-directed self-assembly of organic molecules is one of the most powerful strategies to construct structurally well-defined supramolecular architectures, such as cages,[1-9] macrocycles,[6,7,10,11] and helices.[1,12-18] Some of them can be transformed into other different structures and conformations including the inversion of the helicity[19-21] in response to external stimuli thanks to their dynamic coordination bonds.[22] Among such self-assembled dynamic supramolecules, double- and triple-stranded helicates formed through metal coordination-driven self-assembly have become one of the most fascinating and popular structural motifs since the seminal work by Lehn and coworkers.[12] This is because double- and triple-stranded helicates resemble biological helices, such as the DNA double-helix and the collagen triple-helix, and further possess potentials for developing intelligent molecular machines with nanomechanical functions, such as stimuli-responsible molecular springs showing reversible extension and contraction motions.[23-36] Helicates with a controlled handedness also have the potential as a promising asymmetric catalyst.[37] In contrast to the state-of-the-art asymmetric supramolecular catalysts,[38] there are only a few examples of optically active helicate-based asymmetric catalysts, which consist of enantiopure ligands coordinating to transition metals.[39-41]

In early studies, we reported a series of unique spiroborate-based helicates,[29-33,37] such as a double-stranded *racemo* (*rac*)-helicate (*rac*-$\mathbf{DH1_{BNaB}}^-\cdot Na^+$) composed of two anionic spiroborate groups doubly bridged by two *ortho*-linked tetraphenol strands with a biphenylene unit in the middle. The negatively-charged helicate encapsulates a Na^+ ion within its central cavity, thereby forming a contracted helicate (Figure 1a).[29] The central Na^+ ion embedded within the contracted helicate can be replaced with other series of monovalent cations, such as alkali metals, Ag^+, and NH_4^+ ions of different sizes. Some of the metal ions (Li^+, Na^+, K^+, and Ag^+) can be completely extracted by the addition of a suitable cryptand as a strong receptor for each metal ion, which enables the formation of the dianionic extended helicate (*rac*-$\mathbf{DH1_{BB}}^{2-}$), thus leading to extension-contraction motions accompanied by a unidirectional twisting motion upon the release and binding of the monovalent cations (Figure 1a).[32] Recently, we found that a non-helical extended *meso*-helicate (*meso*-$\mathbf{DH1_{BB}}^{2-}\cdot(TBA^+)_2$) (TBA: tetrabutylammonium) quantitatively converted into the contracted *rac*-helicate in the presence of Na^+ ions and water. The Na^+ ions served as a template for stabilizing

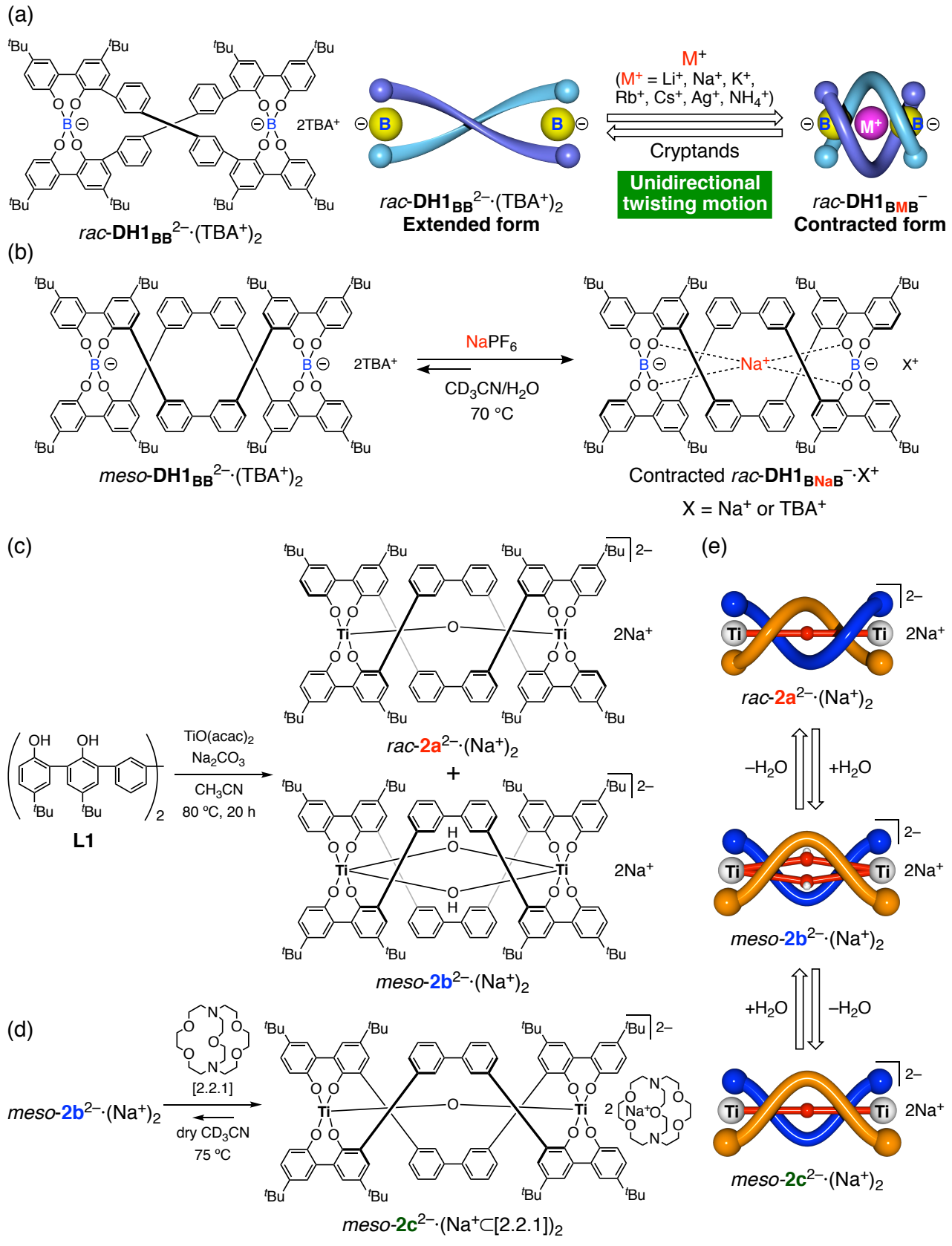

Figure 1. (a) Schematic illustration of the unidirectional spring-like motion of double helical *rac*-$\mathbf{DH1_{BMB}}^{-}$ upon M^+-ion release and binding (M^+ = Li^+, Na^+, K^+, and Ag^+). (b) Na^+-ion-templated conversion of a spiroborate-based double-stranded *meso*-helicate (*meso*-$\mathbf{DH1_{BB}}^{2-}$·$(TBA^+)_2$) into its *racemo*-helicate (*rac*-$\mathbf{DH1_{BNaB}}^{-}$·X^+) (X = Na^+ or TBA^+) in the presence of H_2O. (c) Synthesis of double-stranded titanium(IV) *racemo*- (*rac*-$\mathbf{2a}^{2-}$·$(Na^+)_2$) and *meso*- (*meso*-$\mathbf{2b}^{2-}$·$(Na^+)_2$) helicates. (d) Transformation between *meso*-$\mathbf{2b}^{2-}$·$(Na^+)_2$ and *meso*-$\mathbf{2c}^{2-}$·$(Na^+)_2$ in the absence of H_2O and presence of cryptand [2.2.1]. (e) Schematic illustration of water-mediated reversible three-state structural changes between titanium(IV) *meso*- and *racemo*-helicates upon heating or cooling.

the contracted *rac*-helicate during a reversible water-mediated B–O bond cleavage/reformation reaction that occurred at the spiroborate moieties (Figure 1b).[32]

Considering the characteristic structure of *rac*-$\mathbf{DH1_{BNaB}}^{-}\cdot Na^{+}$ consisting of two spiroborate residues doubly bridged by two tetraphenol strands (**L1**, Figure 1c), we envisioned that the two borate ions would be replaced by titanium (Ti(IV)) ions, thus forming similar dinuclear Ti(IV)-bound *rac*- and/or *meso*-helicates. This working hypothesis is supported by the facts that a large number of double- and triple-stranded dinuclear Ti(IV) *rac*- and *meso*-helicates and helicate-like Ti(IV) complexes has already been prepared mostly using oligomers of phenol derivatives or its analogues including catechol, aminophenol, and benzene-*o*-dithiol linked by non-aromatic flexible linkers as ligands.[1,16,21,42-51] However, dinuclear Ti(IV) helicates composed of fully aromatic oligophenol ligands like **L1** are limited to a few examples.[52-54] The structures of the double-stranded dinuclear Ti(IV) helicates synthesized to date are primarily different from typical helicates self-assembled from oligomers of bipyridine with copper(I), iron(II), etc., such that the two Ti(IV) ions are often linked by one or two bridging ligands, such as μ-oxo,[55,56] μ-hydroxo,[45,48] and μ-alkoxy groups.[48,49,57]

Hiratani and coworkers reported an intriguing water-mediated transformation of a mono-μ-oxo bridged Ti(IV) *rac*-helicate composed of Schiff base dimers into its bis(μ-oxo) bridged *meso*-helicate as revealed by X-ray crystal structures, which was, however, not reversible and their structures in solution were not elucidated because of their high sensitivity to moisture.[55] On the other hand, Albrecht and coworkers reported a series of structurally well-defined double- and triple-stranded Ti(IV) helicates[16,17,42,44,47-49,58,59] and recently demonstrated an elegant example of an ion-triggered three-state, stereochemical molecular switch of a triple-stranded dinuclear Ti(IV) helicate consisting of three optically-active bis(catechol) ligands, showing reversible inversion of the helicity coupled with the elastic motion of the helicate.[21] Surprisingly, however, there are no examples of optically-active dinuclear Ti(IV)-based helicates showing an optical activity solely due to their helicity.[18] A large number of optically active Ti(IV)-based helicates has been reported so far, but they are composed of optically pure ligands[21,49,60,61] or induced by chiral additives,[54] resulting in the formation of a thermodynamically stable either a right- or left-handed diastereomeric helicate. This is due to a kinetically labile nature of Ti(IV) ions as reported by Albrecht.[21,44,59]

We now report a unique water-mediated, reversible control of three-state helicates based on unique structural transformations between three discrete double-stranded dinuclear Ti(IV) chiral *rac*- and achiral *meso*-helicates (*rac*-$\mathbf{2a}^{2-}\cdot(Na^{+})_2$, *meso*-$\mathbf{2b}^{2-}\cdot(Na^{+})_2$, and *meso*-$\mathbf{2c}^{2-}\cdot(Na^{+})_2$) possessing a mono-μ-oxo or a bis(μ-hydroxo) linker that bridges the two Ti(IV) ions (Figure 1c,d). This three-state molecular transformation relies on reversible hydration/dehydration reactions that occur between the two Ti(IV) centers or its combination with a water-mediated dynamic cleavage/reformation reaction of the Ti-phenoxide (Ti-OPh) bonds upon heating or cooling (Figure 1e). These reactions are susceptible to the water content in the reaction media. Hence, these structurally well-defined helicates can be transformed into one another in a selective manner by only changing the water content. Although a number of stimuli-responsive/triggered reversible structural transformations has been reported in polymeric and supramolecular helical systems,[21,29,37] reversible multiple transformation of helical systems controlled by a water content is unique and has not been reported. We also describe the first isolation of an optically active dinuclear Ti(IV)-based helicate composed of achiral components and reversible transformations between the *rac*-$\mathbf{2a}^{2-}\cdot(Na^{+})_2$ and *meso*-$\mathbf{2b}^{2-}\cdot(Na^{+})_2$ helicates that are possible using a catalytic amount of an acid at lower temperature.

RESULTS AND DISCUSSION

Synthesis of Double-Stranded Dinuclear Helicates. The reaction of the tetraphenol ligand **L1** with titanium(IV)oxide bis(acetylacetonate) ($TiO(acac)_2$) (1 equiv) in the presence of sodium carbonate (1 equiv) in CH_3CN at 80 °C under N_2 afforded a crude mixture of $\mathbf{2a}^{2-}\cdot(Na^{+})_2$ and $\mathbf{2b}^{2-}\cdot(Na^{+})_2$, which were then purified and isolated as a yellow solid by the combination of repetitive filtration and reprecipitation/recrystallization procedures (Scheme S1) (for more details, see the Supporting Information (SI)). The isolated helicates $\mathbf{2a}^{2-}\cdot(Na^{+})_2$ and $\mathbf{2b}^{2-}\cdot(Na^{+})_2$ were characterized and identified by ^{1}H and ^{13}C NMR (Figures S2 and S3), single-crystal X-ray diffraction (Figures S19 and S20), and cold-spray ionization (CSI) mass spectrometry (Figure S6) analyses.

Structural Analysis of $\mathbf{2a}^{2-}$ and $\mathbf{2b}^{2-}$ Helicates. The *racemo*-structure of $\mathbf{2a}^{2-}$ was determined by the X-ray crystallographic analysis of the single crystals of $\mathbf{2a}^{2-}\cdot((S)\text{-}\mathbf{3}^{+})_2$ ($\mathbf{3}^{+}$: *N*,*N*,*N*-trimethyl-1-(naphthalene-1-yl)ethan-1-ammonium) obtained by slow evaporation of a solution of $\mathbf{2a}^{2-}\cdot(Na^{+})_2$ with a large excess of the optically-pure (*S*)-$\mathbf{3}^{+}\cdot I^{-}$ in CH_3CN (Figures 2a and S19), which revealed that $\mathbf{2a}^{2-}\cdot((S)\text{-}\mathbf{3}^{+})_2$ adopts a mixture of double-stranded right- and left-handed *racemic* helical structures with a psudo-D_2-symmetry even in the presence of optically-pure (*S*)-$\mathbf{3}^{+}$ counter cations. The two ligand strands are intertwined with each other bridged by two Ti(IV) ions connected by a single μ-oxo ligand to form an almost linear Ti–O–Ti geometry (bond angle = ca. 175°) with a Ti–Ti distance of 3.6 Å and the twist angle between the two terminal benzene rings of each strand of ca. 269° (Figure 2a and Table 1). The Ti–Ti distance and Ti–O–Ti bond angle observed in the crystal structure of *rac*-$\mathbf{2a}^{2-}$ are almost identical to those of the reported mono-μ-oxo bridged dinuclear Ti(IV) complex.[56]

In contrast to the double-helical structure of *rac*-$\mathbf{2a}^{2-}$, the single-crystal structure of $\mathbf{2b}^{2-}\cdot(Na^{+})_2$ showed a non-helical double-stranded *meso*-structure with an approximate C_{2h}-symmetry, in which the two Ti(IV) ions are doubly bridged by two μ-hydroxo groups to form a rhombic four-membered $[Ti_2(\mu\text{-}OH)_2]$ ring in the core and each Na^{+} ion is coordinated by three oxygen atoms of the μ-OH and two phenoxide groups (Figures 2b and S20). Because of the bis(μ-hydroxo) bridged *meso*-structure of $\mathbf{2b}^{2-}\cdot(Na^{+})_2$ with a mirror plane, the configurations (Δ or Λ) of the hexa-coordinated Ti(IV) stereocenters are opposite to each other. The two biphenylene units in the middle of the strands take a nearly planar conformation (ca ±5.0°) and are parallel to each other. Hence, the twist angle between the two terminal benzene rings of each strand is almost zero (±1°). The Ti–Ti distance and Ti–O–Ti bond angle of *meso*-$\mathbf{2b}^{2-}\cdot(Na^{+})_2$ are ca. 3.4 Å and 111°, respectively (Table 1), whereas those of the analogous double-stranded dinuclear Ti(IV) complexes linked by a bis(μ-OR) bridge (R = H,[45,48] none,[55] or alkyl[48,49,57]) are varied depending on their structural rigidity and/or bulkiness of the component strands.

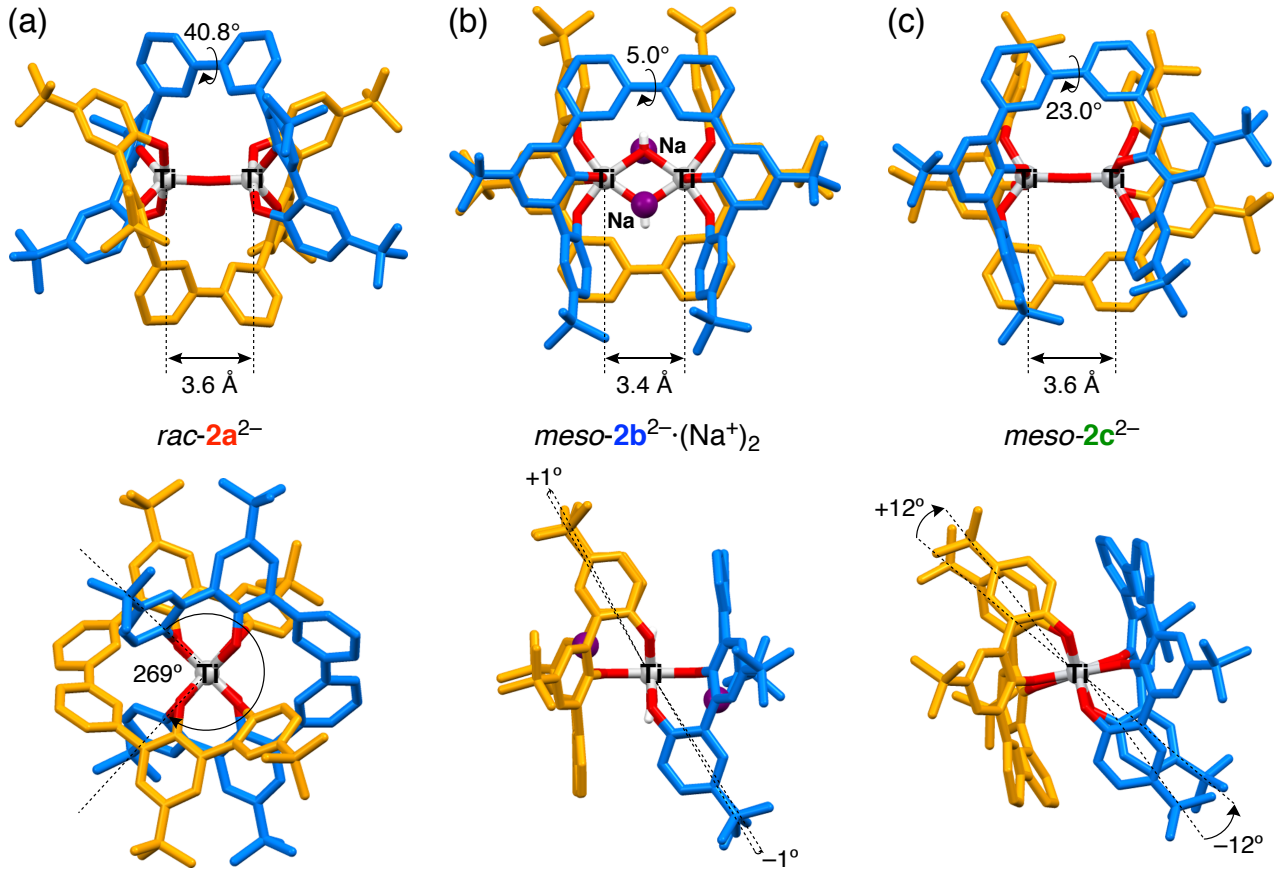

Figure 2. Capped-stick representations of the X-ray crystal structures of *rac*-**2a**$^{2-}$·((*S*)-**3**$^{+}$)$_2$ (a) and *meso*-**2b**$^{2-}$·(Na^{+})$_2$ (b) and the energy-minimized structure of *meso*-**2c**$^{2-}$ (c) obtained by the DFT calculation (side and top (bottom) views). All the hydrogen atoms, ammonium cations (a), and solvent molecules are omitted for clarity.

Table 1. Bond Distances ($d_{B\text{-}B}$ or $d_{Ti\text{-}Ti}$) between Two Boron or Titanium Atoms, Bond Angles, Dihedral Angles, and Twist Angles of the Crystal Structures of Right-Handed (*P*)-*rac*-DH1**$_{BNaB}^{-}$, *meso*-**DH1**$_{BNaB}^{2-}$, (*P*)-*rac*-**2a**$^{2-}$, and *meso*-**2b**$^{2-}$ and the DFT-Calculated Energy-Minimized Structures of (*P*)-*rac*-**2a**$^{2-}$, *meso*-**2b**$^{2-}$, *meso*-**2c**$^{2-}$, and (*P*)-*rac*-**2d**$^{2-}$**

helicate	method	$d_{B\text{-}B}$ or $d_{Ti\text{-}Ti}$ (Å)	bond angle (deg)	dihedral angle (deg)	twist angle (deg)[a]
contracted *rac*-**DH1**$_{BNaB}$[b]	X-ray	6.0[b]	–	42.8[c,d]	285[c]
extended *meso*-**DH1**$_{BB}^{2-c}$	X-ray	11.8[d]	–	79.9[c,d]	±17.5[c]
rac-**2a**$^{2-}$·((*S*)-**3**)$_2$	X-ray	3.6	175[e]	40.8[f]	269
meso-**2b**$^{2-}$·(Na^{+})$_2$	X-ray	3.4	111[g]	5.0[f]	±1
rac-**2a**$^{2-h}$	[DFT]	[3.6][i]	[179][e,i]	[43.3][f,i]	[265][i]
meso-**2b**$^{2-h}$	[DFT]	[3.3][i]	[110][gij]	[15.4][f,i]	[±5][i]
meso-**2c**$^{2-h}$	[DFT]	[3.6][i]	[176][f,i]	[23.0][f,i]	[±12][i]
rac-**2d**$^{2-h}$	[DFT]	[3.3][i]	[108][g,i]	[57.4][f,i]	[295][i]

[a]Twist angles between the two terminal benzene rings (R1 and R6, Ra and Rf) of each strand (see Table S3). [b]Taken from ref 29. [c]Taken from ref 32. [d]Average absolute values. [e]Absolute values of Ti_1-O_5-Ti_2. [f]Average absolute values of R3-R4 and Rc-Rd. [g]Average absolute values of Ti_1-O_5-Ti_2 and Ti_1-Oe-Ti_2. [h]DFT calculations were carried out without a non-entrapped counter cation. [i]The values in parentheses were obtained from the DFT-calculated structures. For more detailed structural data, see Table S4.

All of the reported bis(μ-OR) bridged dinuclear metal complexes and dimers of mononuclear complexes are reported to adopt a *meso*-structure with the opposite configurations at the metal stereocenters to each other,[45,48,49,55,57] whereas the mono-μ-oxo bridged dinuclear metal complexes adopt either a *rac*- or *meso*-structure.[55,56] The observed *meso*-structure preference for the bis(μ-OR)-bound metal complexes is most likely due to a hexa-coordinated, octahedral geometry around the two bis(μ-OR) bridged metal ions, thereby forming an energetically-favorable *meso*-structure.

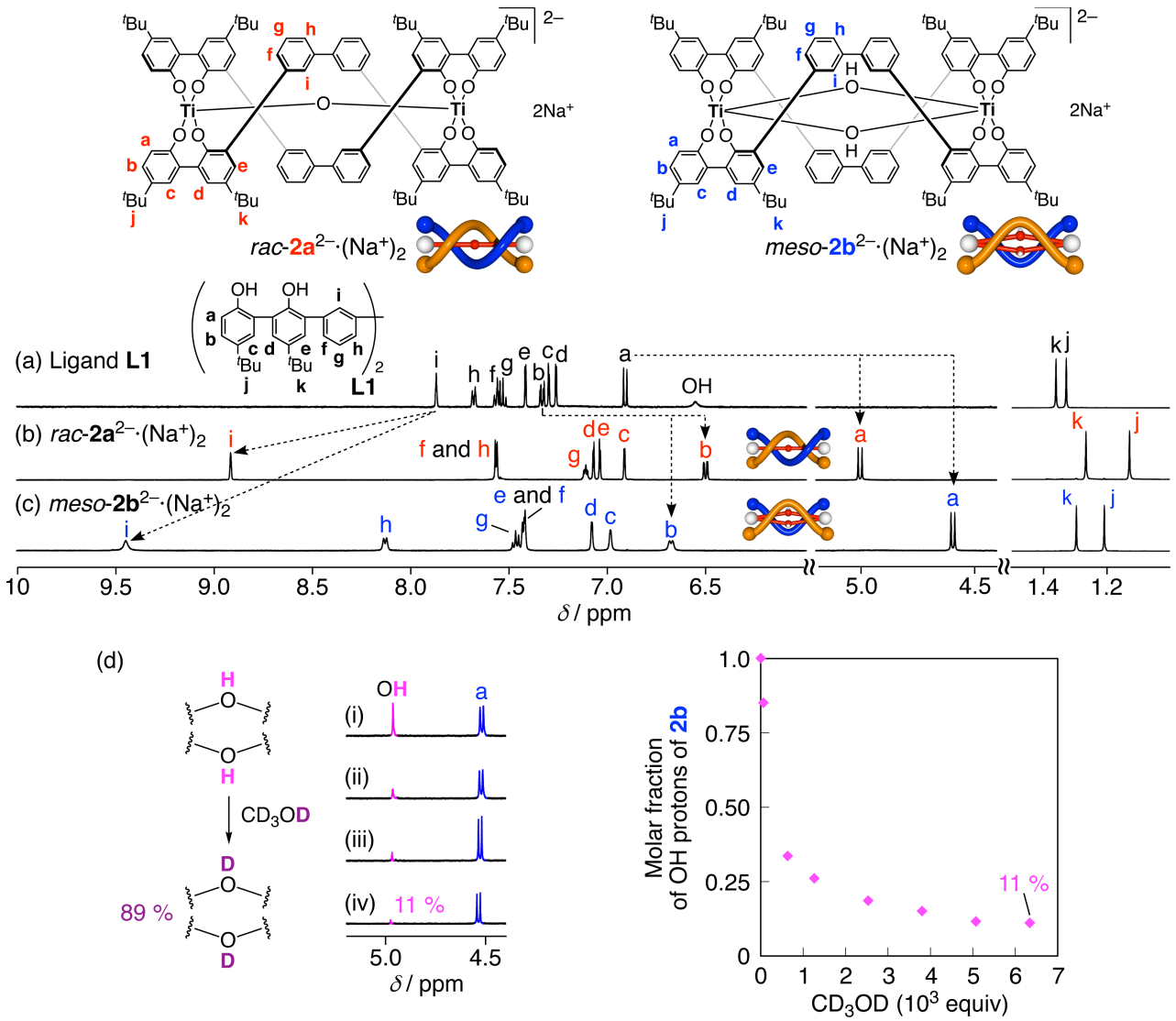

Figure 3. (a-c) ^{1}H NMR spectra (500 MHz, CD_3CN, 0.50 mM, 25 °C) of **L1** (a), *rac*-**2a**$^{2-}$·$(Na)_2$ (b), and *meso*-**2b**$^{2-}$·$(Na)_2$ (c). (d) ^{1}H NMR spectral changes of the bridged μ-hydroxo (OH) protons of *meso*-**2b**$^{2-}$·$(Na^+)_2$ (500 MHz, DMSO-d_6 containing > ca. 130 equiv of H_2O, 0.5 mM, rt) due to hydrogen/deuterium (H/D) exchange in the presence of an increasing amount of CD_3OD: $[CD_3OD]/[meso\text{-}\mathbf{2b}^{2-}\cdot(Na^+)_2]_0 = 0$ (i), 634 (ii), 2530 (iii), and 6340 (iv) (top). Plot of the molar fraction of the bridged μ-hydroxo (OH) protons of *meso*-**2b**$^{2-}$·$(Na^+)_2$ versus $[CD_3OD]/[meso\text{-}\mathbf{2b}^{2-}\cdot(Na^+)_2]_0$ (0–6340 equiv).

These observations are in good agreement with the present *rac*-**2a**$^{2-}$ and *meso*-**2b**$^{2-}$ helicate structures.

The high-resolution negative mode CSI mass spectra of *rac*-**2a**$^{2-}$·$(Na^+)_2$ and *meso*-**2b**$^{2-}$·$(Na^+)_2$ exhibited molecular peaks due to the monovalent anions of $[\mathbf{2a}^{2-} + Na^+]^-$ and $[\mathbf{2b}^{2-} + Na^+]^-$ centered at *m*/*z* 1619.89 and 1637.90, respectively, with approximately 18 (*m*/*z*) mass difference corresponding to one water molecule (Figure S6). These results support the mono-μ-oxo and bis(μ-hydroxo) bridged *rac*-**2a**$^{2-}$ and *meso*-**2b**$^{2-}$ helicate structures, respectively, which were retained in solution.

The ^{1}H NMR spectra of *rac*-**2a**$^{2-}$·$(Na^+)_2$ and *meso*-**2b**$^{2-}$·$(Na^+)_2$ in CD_3CN displayed one set of signals due to their pseudo-D_2- and C_{2h}-symmetric structures, respectively, as expected from their crystal structures (Figure 3b,c). However, the bridged μ-hydroxo (OH) protons of *meso*-**2b**$^{2-}$·$(Na^+)_2$ could not be observed probably because of significant broadening of the OH protons due to a relatively slow exchange between the coordinated and dissociated Na^+ ion species in CD_3CN on the NMR time scale (Figure 3c). In fact, the bridged μ-OH signals appeared as a sharp singlet at 4.96 ppm in DMSO-d_6 and CD_3CN in the presence of cryptand [2.2.1] (4 equiv), which trapped the Na^+ ions, resulting in the complete release of the Na^+ ions from the *meso*-**2b**$^{2-}$. The peak intensity of the bridged μ-OH decreased with the increasing amount of CD_3OD in DMSO-d_6 due to the hydrogen/deuterium (H/D) exchange and did not change in the presence of a large excess amount of CD_3OD after 66.5 h, while the other signals remained unchanged (Figures 3d and 6a).

The aromatic protons (H_a and H_b) on the terminal benzene rings of the *rac*-**2a**$^{2-}$ and *meso*-**2b**$^{2-}$ helicates were significantly shifted upfield as compared to those of the corresponding ligand **L1** due to the ring current effect of the phenyl rings of the biphenyl linker of the other strand (Figure 3a-c). In contrast, the aromatic protons (H_i) at the *ortho*-position of the biphenyl linkers were shifted downfield most likely due to the $CH_i\cdots O$ hydrogen bonds with the oxygen atom of the terminal benzene ring of the other strand for *rac*-**2a**$^{2-}$·$(Na^+)_2$ (H···O distance =

2.8 Å) and those with the oxygen atom of the adjacent benzene ring of the same strand for *meso*-$\mathbf{2b}^{2-}\cdot(Na^+)_2$ (H···O distance = 2.3 – 2.4 Å)[62] (Figures 3a-c and S22a,b) (for complete signal assignments, see COSY and NOESY spectra (Figures S23−S27 for *rac*-$\mathbf{2a}^{2-}\cdot(Na^+)_2$ and Figures S28−S34 for *meso*-$\mathbf{2b}^{2-}\cdot(Na^+)_2$)). These observations are consistent with their crystal and density functional theory (DFT) calculated structures (Figures 2a,b, S21a,b, and S22a,b).

Thermal Transformation between *Racemo*-$\mathbf{2a}^{2-}$ and *Meso*-$\mathbf{2b}^{2-}$ Helicates. Comparison of the structures of *rac*-$\mathbf{2a}^{2-}\cdot(Na^+)_2$ and *meso*-$\mathbf{2b}^{2-}\cdot(Na^+)_2$ with an approximate 18 (*m*/*z*) mass difference indicated a reversible water-mediated transformation between *rac*-$\mathbf{2a}^{2-}\cdot(Na^+)_2$ and *meso*-$\mathbf{2b}^{2-}\cdot(Na^+)_2$ would be possible through hydration/dehydration reactions, which requires cleavage/reformation of the Ti-OPh bonds catalyzed by water because of rearrangement of the coordination geometry of the Ti(IV) ions. We envisioned that such a water-mediated transformation between *rac*-$\mathbf{2a}^{2-}\cdot(Na^+)_2$ and *meso*-$\mathbf{2b}^{2-}\cdot(Na^+)_2$ can be controlled in a switch-like manner by a change in the water content in the reaction media. In fact, when a solution of *meso*-$\mathbf{2b}^{2-}\cdot(Na^+)_2$ in CD_3CN in the presence of ca. 10 equiv of water was heated to 75 °C,[63] the *meso*-$\mathbf{2b}^{2-}\cdot(Na^+)_2$ was gradually converted to the *rac*-$\mathbf{2a}^{2-}\cdot(Na^+)_2$, reaching an almost equilibrium state after 330 min (*meso* : *racemo* = 22:78) (Figures 4B, Da, and S7). The forward (k) and reverse (k_{-1}) reaction rate constants were estimated to be 1.15×10^{-4} and 2.38×10^{-5} s^{-1}, respectively, based on the nonlinear least-squares curve fitting of the NMR spectral changes, leading to an equilibrium constant ($K = k_1/k_{-1} = 4.83$). The *meso* : *racemo* ratio was then calculated to be 17:83 at equilibrium, which is reasonably consistent with the observed ratio (22:78) (Figure 4D). As a result, the achiral *meso*-$\mathbf{2b}^{2-}\cdot(Na^+)_2$-to-chiral *rac*-$\mathbf{2a}^{2-}\cdot(Na^+)_2$ configurational transformation took place through dehydration coupled with a water-mediated cleavage/reformation of the covalent Ti-OPh bonds catalyzed by a slight excess of water in CD_3CN with neither no byproduct formation nor decomposition (Figure 4B).

In the presence of a large excess of water (>1000 equiv of water), the *rac*-$\mathbf{2a}^{2-}\cdot(Na^+)_2$ was readily transformed into *meso*-$\mathbf{2b}\cdot(Na^+)_2$ through hydration accompanied by the Ti-OPh bond cleavage/reformation in CD_3CN at 75 °C, reaching an equilibrium within 30 min (*racemo* : *meso* = 12:88) (Figure 4C). At 25 °C, however, *rac*-$\mathbf{2a}\cdot(Na^+)_2$ was resistant to transformation even in the presence of more than 1000 equiv of water, mostly due to the high activation energy barrier for the *rac*-$\mathbf{2a}\cdot(Na^+)_2$-to-*meso*-$\mathbf{2b}^{2-}\cdot(Na^+)_2$ transformation (Figure S8). Hence, the formation of *rac*-$\mathbf{2a}^{2-}\cdot(Na^+)_2$ and *meso*-$\mathbf{2b}^{2-}\cdot(Na^+)_2$ can be controlled by changing an amount of water in the reaction media upon heating.

Another *rac*-helicate bridged by a bis(μ-hydroxo) unit (*rac*-$\mathbf{2d}^{2-}\cdot(Na^+)_2$) (Figure 4A) could be generated in principle during the hydration of the mono-μ-oxo-bridged *rac*-$\mathbf{2a}^{2-}\cdot(Na^+)_2$ while keeping its double-helical *racemo*-framework. However, the formation of *rac*-$\mathbf{2d}^{2-}\cdot(Na^+)_2$ was not observed at all during the *rac*-$\mathbf{2a}^{2-}\cdot(Na^+)_2$-to-*meso*-$\mathbf{2b}^{2-}\cdot(Na^+)_2$ transformation at 25 and 75 °C in aqueous CD_3CN independent of the amount of water (Figures 4C and S8). The DFT calculated structures of a series of Ti(IV) helicates revealed that *rac*-$\mathbf{2d}^{2-}$ is 14.9 kcal/mol more unstable than the corresponding *meso*-$\mathbf{2b}^{2-}$ helicate probably due to its distorted doubly μ-hydroxo-bridged *racemo*-structure of *rac*-$\mathbf{2d}^{2-}$; all atoms of the Ti–$(OH)_2$–Ti unit of *meso*-$\mathbf{2b}^{2-}$ are approximately on the same plane (Figure S21b), whereas the Ti–$(OH)_2$–Ti unit of *rac*-$\mathbf{2d}^{2-}$ is disordered to retain its *racemo*-framework so that the two bridged μ-hydroxo (OH) bonds bend out of the Ti–O_2–Ti unit plane due to the steric repulsion with the neighboring biphenyl residues (Figure S21d), resulting in more twisted conformations of the central biphenyl residues (57.4°) than those of the *meso*-$\mathbf{2b}^{2-}$ (15.4° (DFT calculated structure) and 5.0° (X-ray structure)) (see dihedral angle in Table 1).

In strong contrast to the spiroborate-based *racemic* helicates, such as *rac*-$\mathbf{DH1_{BNaB}}^-\cdot Na^+$,[29-32] various attempts to resolve the racemic Ti(IV) helicate *rac*-$\mathbf{2a}^{2-}\cdot(Na^+)_2$ into the enantiomers by conventional diastereomeric salt formation using a variety of optically-pure ammonium salts, such as (*S*)-$\mathbf{3}^+\cdot I^-$ and *N*-benzylquininium chloride ($QN^+\cdot Cl^-$), produced only diastereomeric crystals of racemic $\mathbf{2a}^{2-}$ (Figure 2a) as already described. This is probably because of racemization catalyzed by water contained in the used solvent that rapidly took place during the optical resolution process. We note that racemization or interconversion between the right- and left-handed double-helical enantiomers of $\mathbf{2a}^{2-}$ requires simultaneous cleavages of one of the four Ti–OPh bonds at each Ti(IV) center probably by the formation of an achiral *meso* intermediate (*meso*-$\mathbf{2b}^{2-}$), followed by reforming of the right- or left-handed helicate ($\mathbf{2a}^{2-}$) (Figure S49)

We then followed the ^1H NMR spectral changes of *meso*-$\mathbf{2b}^{2-}\cdot(Na^+)_2$ in the presence of 5 equiv of $QN^+\cdot Cl^-$ in CD_3CN containing a moderate amount of water (64 equiv) at 25 °C with the expectation that the *meso*-$\mathbf{2b}^{2-}\cdot(Na^+)_2$-to-*rac*-$\mathbf{2a}^{2-}\cdot(Na^+)_2$ transformation could proceed in a helix-sense selective manner, thereby producing an optically-active $\mathbf{2a}^{2-}\cdot(Na^+)_2$ with an excess of either a right- or left-handed double-helical structure in solution induced by the QN^+ cations (Figure S50). The aromatic ($H_{c'}$ and $H_{d'}$) and *t*-Bu ($H_{k'}$) protons of *meso*-$\mathbf{2b}^{2-}\cdot(Na^+)_2$ split into two sets of nonequivalent signals with an equal intensity by the addition of the optically-pure $QN^+\cdot Cl^-$ because of its double-stranded *meso*-structure composed of mirror-imaged Ti(IV) stereocenters (Δ and Λ) in the molecule, and therefore, the aromatic and *t*-Bu protons become diastereotopic upon complexation with the optically-pure QN^+ (Figure S50b,c). After storing the complex solution at room temperature for 4 days, 36% of the *meso*-$\mathbf{2b}^{2-}$ was converted to the double-helical $\mathbf{2a}^{2-}$ that also displayed two sets of proton signals (H_e and H_k) with an approximately equal intensity due to the formation of a pair of diastereomers composed of right- and left-handed double-helices of $\mathbf{2a}^{2-}$ complexed with QN^+ (Figure S50a,d), indicating that the double-helical $\mathbf{2a}^{2-}$ exists as a racemic mixture, as further supported by no circular dichroism (CD) signal in the Ti(IV) helicate chromophore region. These results indicated that the optically-pure QN^+ could not assist the helix-sense-selective formation of an optically-active $\mathbf{2a}^{2-}$ during the water catalyzed transformation from achiral *meso*-$\mathbf{2b}^{2-}$.

We then attempted direct enantioseparation of *rac*-$\mathbf{2a}^{2-}\cdot(Na^+)_2$ by HPLC[64-66] using a series of chiral columns (Daicel, Osaka, Japan) under a variety of normal and reversed phase eluent conditions with UV and CD dual detectors. However, all attempted separations of *rac*-$\mathbf{2a}^{2-}\cdot(Na^+)_2$ resulted in mostly single peaks with negligible CD intensity. The reason for this is not clear at present. However, during the chromatographic enantioseparation of *rac*-$\mathbf{2a}^{2-}\cdot(Na^+)_2$, we observed significant tailing and fronting of a chromatographic peak when CHIRALPAK IA (Daicel, Osaka, Japan) was used as

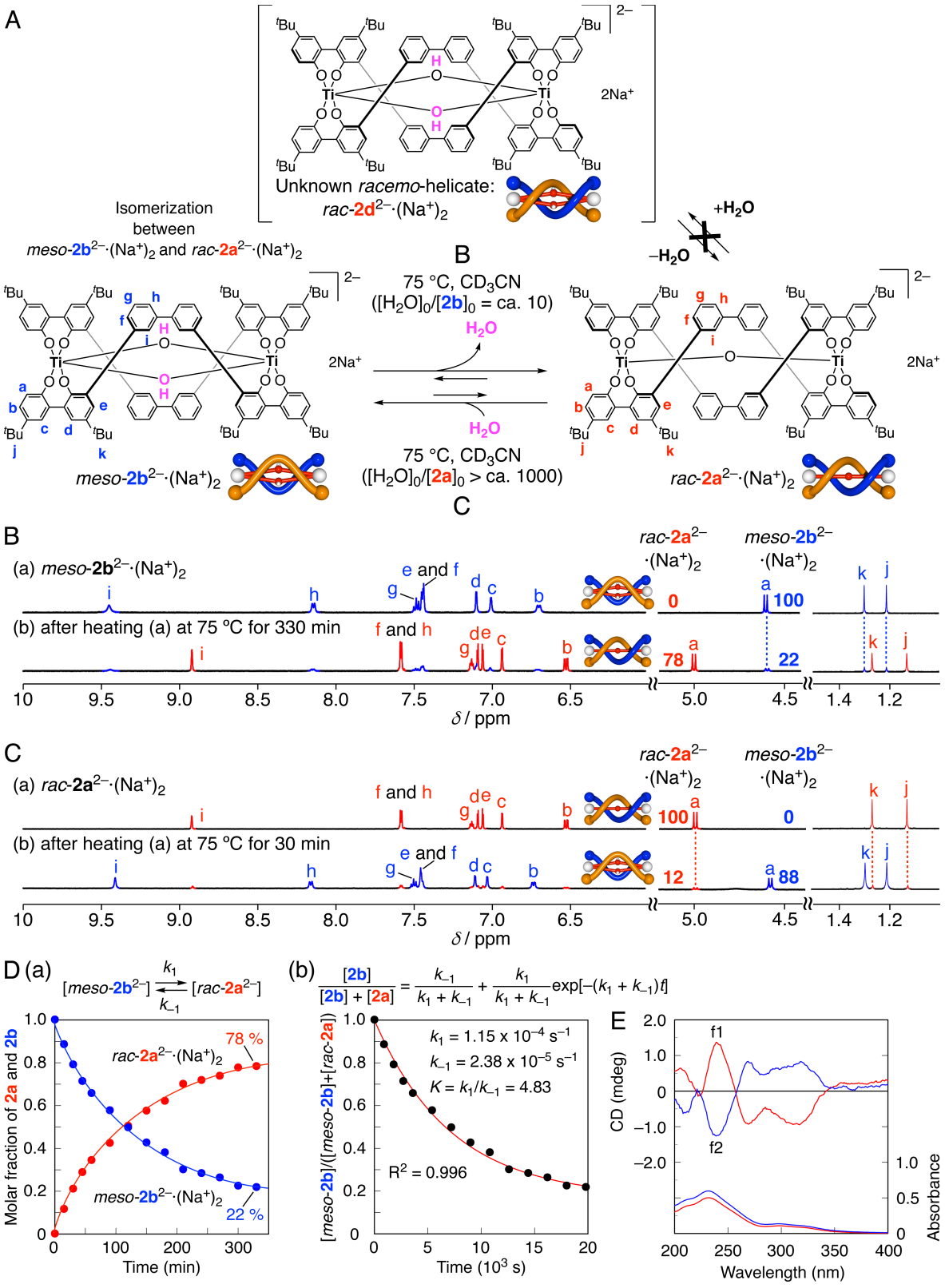

Figure 4. (A) Structure of an unknown doubly μ-hydroxo-bridged *racemo*-helicate (*rac*-**2d**$^{2-}$·(Na$^+$)$_2$). (B) ^{1}H NMR spectra of *meso*-**2b**$^{2-}$·(Na$^+$)$_2$ (500 MHz, CD_3CN containing H_2O ([H_2O]$_0$/[*meso*-**2b**$^{2-}$.(Na$^+$)$_2$]$_0$ = ca. 10), 0.50 mM) measured at 25 °C before (a) and after heating at 75 °C for 330 min (b). (C) ^{1}H NMR spectra of *rac*-**2a**$^{2-}$·(Na$^+$)$_2$ (500 MHz, CD_3CN containing H_2O ([H_2O]$_0$/[*rac*-**2a**$^{2-}$·(Na$^+$)$_2$]$_0$ > ca. 1000), 0.49 mM) before (a) and after heating at 75 ºC for 30 min (b), measured at 25 °C. (D) (a) Plots of the molar fractions of *meso*-**2b**$^{2-}$·(Na$^+$)$_2$ and *rac*-**2a**$^{2-}$·(Na$^+$)$_2$ as a function of time during the *meso*-**2b**$^{2-}$-to-*rac*-**2a**$^{2-}$ transformation, estimated by ^{1}H NMR spectral changes (see Figure S7). The solid lines are drawn to guide the eyes. (b) Transformation kinetics of *meso*-**2b**$^{2-}$·(Na$^+$)$_2$. (E) CD and absorption spectra of optically active **2a**$^{2-}$·(Na$^+$)$_2$ (f1 and f2) obtained by chromatographic enantioseparation, measured in CH_3CN at 25 °C (see text and Figure S1).

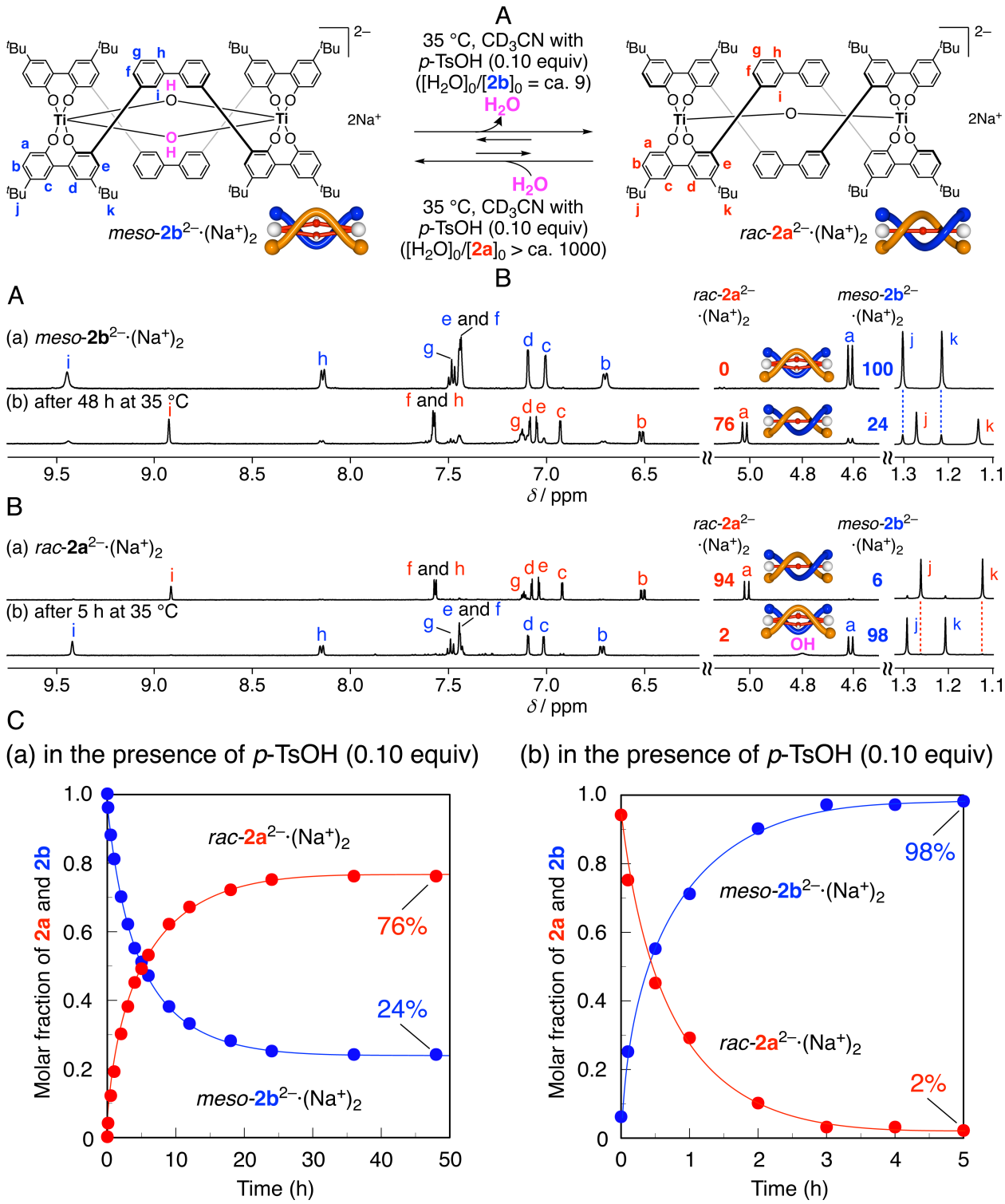

Figure 5. (A) ^{1}H NMR spectra of *meso*-**2b**$^{2-}$·(Na$^+$)$_2$ (500 MHz, CD_3CN containing H_2O ([H_2O]$_0$/[*meso*-**2b**$^{2-}$·(Na$^+$)$_2$]$_0$ = ca. 9), 0.50 mM) in the presence of *p*-TsOH (0.10 equiv) measured at 35 °C before (a) and after heating at 35 °C for 48 h (b). (B) ^{1}H NMR spectra of *rac*-**2a**$^{2-}$·(Na$^+$)$_2$ (500 MHz, CD_3CN containing H_2O ([H_2O]$_0$/[*rac*-**2a**$^{2-}$·(Na$^+$)$_2$]$_0$ > ca. 1000), 0.50 mM) in the presence of *p*-TsOH (0.10 equiv) before (a) and after heating at 35 °C for 5 h (b), measured at 35 °C. (C) (a) Plots of the molar fractions of *meso*-**2b**$^{2-}$·(Na$^+$)$_2$ and *rac*-**2a**$^{2-}$·(Na$^+$)$_2$ as a function of time during the *meso*-**2b**$^{2-}$-to-*rac*-**2a**$^{2-}$ (a) and *rac*-**2a**$^{2-}$-to-*meso*-**2b**$^{2-}$ transformations (b), estimated by ^{1}H NMR spectral changes. The solid lines are drawn to guide the eyes.

a chiral column with CH_3CN as the eluent at 25 °C (Figure S1). We then fractionated the peak into ten fractions and found that several fractions including the fraction 1 (f1) and fraction 2 (f2) showed mirror-imaged CD spectra (Figure 4E). Hence, a pair of optically active **2a**$^{2-}$·(Na$^+$)$_2$ was successfully obtained, although their enantiomeric excess (ee) values were rather low (less than 10% ee) (Figure S1c). The resolved **2a**$^{2-}$·(Na$^+$)$_2$ maintained their optical activities without racemization after

standing in CH_3CN at room temperature for 60 days. To the best of our knowledge, this is the first example of a dinuclear Ti(IV) helicate showing an optical activity solely due to the helicity.[18,54] The mono-μ-oxo bridge between the Ti(IV) ions of the **2a**$^{2-}$ helicate composed of fully aromatic oligophenol ligands most likely contributes to stabilizing its double helical structure, thereby maintaining its optical activity once partially separated into enantiomers.

Acid-Catalyzed Transformation between *Racemo*-2a^{2-} and *Meso*-2b^{2-} Helicates. Recently, we found that the racemization reaction of an optically active spiroborate-based double-stranded helicate bearing a bisporphyrin unit in the middle was remarkably accelerated in aqueous organic solvents in the presence of a catalytic amount of *para*-toluenesulfonic acid (*p*-TsOH), and proceeded below room temperature.[67] Acid-catalyzed transformations between *rac*-**2a**$^{2-}$·$(Na^+)_2$ and *meso*-**2b**$^{2-}$·$(Na^+)_2$ were then investigated in CD_3CN containing an appropriate amount of water as shown in Figure 4 in the presence of a catalytic amount of *p*-TsOH (0.10 equiv) (Figure 5 and Section 5 in the SI). Interestingly, both the *meso*-**2b**$^{2-}$-to-*rac*-**2a**$^{2-}$ and *rac*-**2a**$^{2-}$-to-*meso*-**2b**$^{2-}$ transformations proceeded at 35 °C and reached an equilibrium state within ca. 40 h (*meso* : *racemo* = 24:76) and 5 h (*racemo* : *meso* = 2:98), respectively (Figure 5C). In the absence of *p*-TsOH, each transformation hardly took place or required a much longer time to reach an equilibrium (Figure S18). As a result, the formations of *rac*-**2a**$^{2-}$·$(Na^+)_2$ and *meso*-**2b**$^{2-}$·$(Na^+)_2$ were found to be controlled using a catalytic amount of *p*-TsOH even at lower temperature.

Transformation between the *Meso*-2b^{2-} and *Meso*-2c^{2-} Helicates. The crystal structure of the *meso*-**2b**$^{2-}$·$(Na^+)_2$ revealed that the two Na^+ ions significantly contribute to stabilizing its *meso*-structure through coordination to the oxygen atoms of the μ-OH and phenoxide groups (Figure 2b). We anticipated that if the coordinated Na^+ ions could be removed from *meso*-**2b**$^{2-}$·$(Na^+)_2$ with the assistance of cryptand [2.2.1], the *meso*-**2b**$^{2-}$·$(Na^+)_2$ helicate would more efficiently convert to the *rac*-**2a**$^{2-}$·$(Na^+)_2$ helicate. Surprisingly, however, only a trace amount of *rac*-**2a**$^{2-}$ was produced upon the heating of a solution of *meso*-**2b**$^{2-}$·$(Na^+)_2$ in the presence of cryptand [2.2.1] (4 equiv) and ca. 12 equiv of water in CD_3CN at 75 °C based on its ^{1}H NMR spectrum (Figure S9a,b). Instead, one set of new signals (**2c**$^{2-}$·$(Na^+\subset[2.2.1])_2$) appeared as a minor species within 30 min (*rac*-**2a**$^{2-}$:*meso*-**2b**$^{2-}$:**2c**$^{2-}$ = 1:86:13). The newly generated third helicate (**2c**$^{2-}$·$(Na^+\subset[2.2.1])_2$) was found to readily revert back to the original *meso*-**2b**$^{2-}$·$(Na^+\subset[2.2.1])_2$ after standing at room temperature for 60 min, while the *rac*-**2a**$^{2-}$·$(Na^+\subset[2.2.1])_2$ proton signals remained unchanged (Figure S9c). This result indicated that the observed reversible transformation takes place between *meso*-**2b**$^{2-}$ and **2c**$^{2-}$ via a reversible dehydration/hydration under the present conditions using cryptand [2.2.1] and ca. 12 equiv of water. We then followed the ^{1}H NMR spectral changes of *meso*-**2b**$^{2-}$·$(Na^+)_2$ in the absence of the cryptand [2.2.1] in anhydrous CD_3CN (initial water content = 0.5 equiv) at 75 °C. Interestingly, only **2c**$^{2-}$ was converted from *meso*-**2b**$^{2-}$, reaching an equilibrium within 5 min (*meso*-**2b**$^{2-}$:**2c**$^{2-}$ = 83:17) (Figure S10).

These results indicated that the *meso*-**2b**$^{2-}$·$(Na^+)_2$ and *rac*-**2a**$^{2-}$·$(Na^+)_2$ are almost kinetically inert toward configurational transformation from each other in the absence of water and Na^+ ions, and the Na^+ ions play a crucial role as a counter cation in stabilizing the *meso*-**2b**$^{2-}$ helicate framework, and at the same time, assisting the water-mediated cleavage/reformation of the Ti-OPh coordination bonds of the *meso*-**2b**$^{2-}$ and *racemo*-**2a**$^{2-}$ helicates. Based on these observations together with the high-resolution negative mode CSI mass result (see below), the third **2c**$^{2-}$ helicate can be assigned to a mono-μ-oxo *meso*-helicate, generated from *meso*-**2b**$^{2-}$·$(Na^+)_2$ via dehydration, thereby keeping its *meso*-framework (for further discussion of the structure of the *meso*-**2c**$^{2-}$·$(Na^+)_2$, see below).

The *meso*-**2b**$^{2-}$·$(Na^+)_2$-to-*meso*-**2c**$^{2-}$·$(Na^+)_2$ transformation was then investigated by ^{1}H NMR in anhydrous CD_3CN in the presence of cryptand [2.2.1] in combination with 3A molecular sieves in order to remove the Na^+ ions coordinated to the *meso*-**2b**$^{2-}$ and water generated during the transformation, respectively, which would accelerate the formation of the *meso*-**2c**$^{2-}$ and further enhance the stability of the formed *meso*-**2c**$^{2-}$. Otherwise, the formed *meso*-**2c**$^{2-}$ reverts back to the original *meso*-**2b**$^{2-}$ through a reverse hydration reaction. As expected, upon heating of an anhydrous CD_3CN solution (initial water content = 0.5 equiv) of *meso*-**2b**$^{2-}$·$(Na^+)_2$ in the presence of cryptand [2.2.1] (4 equiv) and 3A molecular sieves at 75 °C for 90 min, the dehydration of *meso*-**2b**$^{2-}$·$(Na^+\subset[2.2.1])_2$ efficiently proceeded to give *meso*-**2c**·$(Na^+\subset[2.2.1])_2$ as the major helicate (**2b**$^{2-}$:**2c**$^{2-}$ = 6:94) (see SI for more detailed experimental procedures). The transformation reached an equilibrium state after 90 min with the apparent rate constants for the forward (k_1) and reverse reactions (k_{-1}) of 1.21×10^{-3} and 1.02×10^{-4} s^{-1}, respectively (Figure S11).

To obtain more convincing evidence for the reversible dehydration and hydration reactions that take place during the transformation between the *meso*-**2b**$^{2-}$ and *meso*-**2c**$^{2-}$, we monitored the changes in the amounts of water relative to its original amount of water contained in an anhydrous CD_3CN solution of *meso*-**2b**$^{2-}$·$(Na^+)_2$ during the transformation. The time-dependent ^{1}H NMR spectral changes of *meso*-**2b**$^{2-}$·$(Na^+)_2$ in anhydrous CD_3CN (initial water content = 0.4 equiv) in the presence of cryptand [2.2.1] (4 equiv) at 75 °C revealed that the molar fraction of the formed *meso*-**2c**$^{2-}$ increased in proportion to the amount of the generated water, thereby decreasing the molar fraction of the *meso*-**2b**$^{2-}$. The *meso*-**2b**$^{2-}$-to-*meso*-**2c**$^{2-}$ transformation reached an equilibrium at 75 °C after 90 min (**2b**$^{2-}$:**2c**$^{2-}$ = 17:83) (Figures 6a,b,d and S12a,c).[68] Upon cooling to 25 °C, the backward *meso*-**2c**$^{2-}$-to-*meso*-**2b**$^{2-}$ transformation slowly took place via hydration, giving a 78:22 mixture of *meso*-**2b**$^{2-}$ and *meso*-**2c**$^{2-}$ helicates after 120 h (Figures 6b,c,e and S12b,d), whereas no trace amount of the *rac*-**2a**$^{2-}$ was directly produced from *meso*-**2c**$^{2-}$. The observed changes in the amounts of the in situ generated and consumed water during the transformations between the *meso*-**2b**$^{2-}$ and *meso*-**2c**$^{2-}$ helicates estimated by ^{1}H NMR are reasonably consistent with the calculated values (Figure S12c,d), clearly indicating that the *meso*-**2c**$^{2-}$·$(Na^+)_2$ is generated by the dehydration of the *meso*-**2b**$^{2-}$·$(Na^+)_2$.

Unfortunately, single crystals of *meso*-**2c**$^{2-}$·$(Na^+\subset[2.2.1])_2$ as well as those of *meso*-**2c**$^{2-}$·$(TBA^+)_2$[69] suitable for an X-ray analysis could not be obtained, but direct evidence for the structure was obtained by CSI mass spectrometry (Figures S15 and S17). The high-resolution negative mode CSI mass spectrum of the *meso*-**2c**$^{2-}$·$(Na^+\subset[2.2.1])_2$ immediately after preparation from the *meso*-**2b**$^{2-}$·$(Na^+\subset[2.2.1])_2$ via dehydration upon heating at 65 °C for 20 h exhibited two kinds of molecular peaks due to the monovalent anions of [*meso*-**2c**$^{2-}$ + Na^+]$^-$

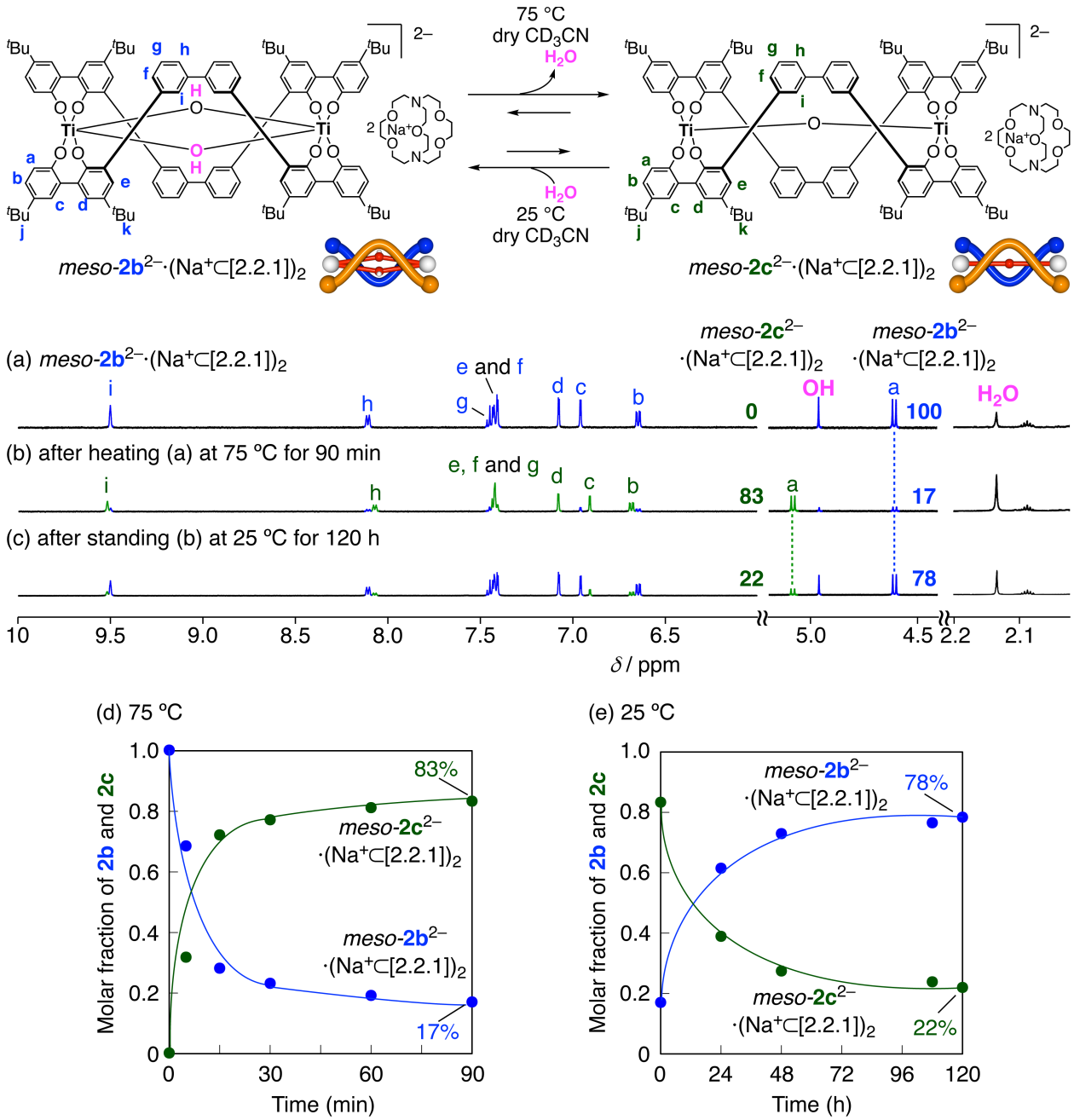

Figure 6. Partial ^{1}H NMR spectra (500 MHz, anhydrous CD_3CN ($[H_2O]_0/[meso\text{-}\mathbf{2b}^{2-}\cdot(Na^+\subset[2.2.1])_2]_0 = 0.40$), 0.50 mM, 25 °C) of *meso*-$\mathbf{2b}^{2-}\cdot(Na^+)_2$ in the presence of 4 equiv of cryptand[2.2.1] before (a) and after heating at 75 °C for 90 min (b) followed by standing at 25 °C for 120 h (c) (for more detailed NMR spectral changes, see Figure S12a,b). Plots of the molar fractions of *meso*-$\mathbf{2b}^{2-}\cdot(Na^+\subset[2.2.1])_2$ and *meso*-$\mathbf{2c}^{2-}\cdot(Na^+\subset[2.2.1])_2$ as a function of time during the transformation at 75 °C (d), followed by standing at 25 °C (e), estimated by ^{1}H NMR spectral changes (see Figure S12a and b, respectively).

and [*meso*-$\mathbf{2b}^{2-}$ + Na^+]$^-$ centered at *m*/*z* 1619.69 and 1637.71, respectively, with approximately 18 (*m*/*z*) mass difference corresponding to one water molecule (Figure S15). Obviously, a small amount of the *meso*-$\mathbf{2b}^{2-}$ was formed through hydration of the *meso*-$\mathbf{2c}^{2-}$ at room temperature (Figure 6e) during the CSI mass measurement. Although the *m*/*z* value of the observed *meso*-$\mathbf{2c}^{2-}$ molecular peak is identical to that of its diastereomer (*rac*-$\mathbf{2a}^{2-}$) (Figure S6a), the *rac*-$\mathbf{2a}^{2-}\cdot(Na^+\subset[2.2.1])_2$ was not produced at all under the present condition as described above. Therefore, we can unequivocally determine the structure of the *meso*-$\mathbf{2c}^{2-}$, which is a diastereomer of the mono-μ-oxo bridged *rac*-$\mathbf{2a}^{2-}$, *i.e.,* the mono-μ-oxo bridged *meso*-$\mathbf{2c}^{2-}$ helicate.

The ^{1}H and ^{13}C NMR spectra provided further useful information that also supports the mono-μ-oxo-bridged *meso*-structure. By comparing the ^{1}H and ^{13}C NMR spectra of the three helicates complexed with $(Na^+\subset[2.2.1])_2$ (Figures S2 and S3), the ^{1}H and ^{13}C NMR spectra of the *meso*-$\mathbf{2b}^{2-}$ and *meso*-$\mathbf{2c}^{2-}$ helicates were very similar to each other because of the same *meso*-framework,[70] in particular those of the biphenylene linker units (H_f – H_i protons in Figure S2 and C ring carbons in Figure S3), except for the aromatic protons (H_a) and carbons (A_2 in ring A) at the *ortho*-position

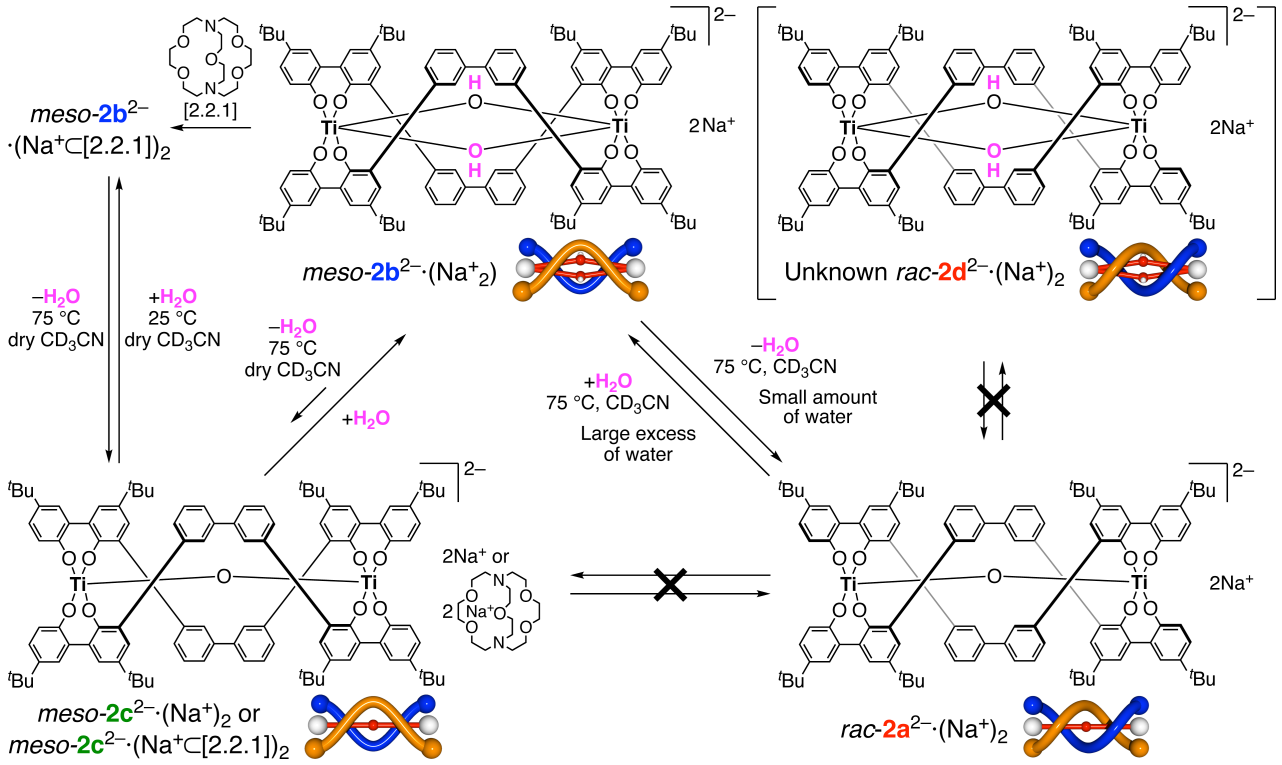

Figure 7. Schematic illustrations of water-mediated reversible three-state structural changes between *rac*-**2a**$^{2-}$·$(Na^+)_2$, *meso*-**2b**$^{2-}$·$(Na^+)_2$, and *meso*-**2c**$^{2-}$·$(Na^+\subset[2.2.1])_2$ helicates.

of the terminal benzene rings of the strands (Figures S2 and S3; for complete proton signal assignments for *meso*-**2c**$^{2-}$·$(Na^+\subset[2.2.1])_2$, see COSY and NOESY spectra (Figures S35–S39) and for complete ^{13}C signal assignments, see HSQC and HMBC spectra (Figures S47 and S48)), whose proton and carbon chemical shifts were rather similar to those of the *rac*-**2a**$^{2-}$, probably due to the same mono-μ-oxo-bridged structure.

The DFT calculated structure of *meso*-**2c**$^{2-}$ displayed a slightly twisted conformation with the twist angle of ±12° (Table 1) as compared to the crystal and DFT calculated structures of *meso*-**2b**$^{2-}$ (twist angle = ±1° and ±5°, respectively) when viewed from the Ti–Ti axis (Figures 2b,c and S21b,c and Table 1). This is due to the increased rotational flexibility of the linear Ti–O–Ti bridge of the *meso*-**2c**$^{2-}$ with the Ti–O–Ti bond angle of ca. 176° and the Ti–Ti distance of 3.6 Å (Table 1), whereas the molecular motion of the Ti–$(OH)_2$–Ti unit in the *meso*-**2b**$^{2-}$ is highly restricted due to the bis(μ-hydroxo) bridge. Therefore, the two biphenylene units in the middle of the strands of *meso*-**2c**$^{2-}$ also take a more twisted conformation (ca ±23°), so that the aromatic H_a protons and the corresponding A_2 carbons of *meso*-**2c**$^{2-}$ were likely affected by the ring current effect of the aromatic rings of the biphenyl linker of the other strand in a similar extent as the *rac*-**2a**$^{2-}$ (Figures S21a-c and S22).[71]

Transformation between *Rac*-2a^{2-}, *Meso*-2b^{2-}, and *Meso*-2c^{2-} Helicates: Control of Three-State Helicates. As already discussed, the reversible transformation between the three discrete *rac*-**2a**$^{2-}$, *meso*-**2b**$^{2-}$, and *meso*-**2c**$^{2-}$ helicates is significantly dependent on the water content in the reaction media, thereby enabling the control of three-state in a switch-like manner by changing the water content upon heating or cooling (Figure 7). At a high concentration of water, *rac*-**2a**$^{2-}$·$(Na^+)_2$ can be selectively transformed into *meso*-**2b**$^{2-}$·$(Na^+)_2$ through hydration accompanied by the water-mediated Ti-OPh bond cleavage/reformation upon heating, whereas the corresponding structural isomer of *meso*-**2b**$^{2-}$·$(Na^+)_2$, *i.e.*, *rac*-**2d**$^{2-}$·$(Na^+)_2$, was not produced at all because of its sterically hindered, doubly μ-hydroxo-bridged *racemo*-structure as supported by the DFT calculations (Figure S21). On the other hand, *meso*-**2b**$^{2-}$·$(Na^+)_2$ readily converts to *rac*-**2a**$^{2-}$·$(Na^+)_2$ in the presence of a moderate amount of water upon heating through dehydration coupled with the Ti-OPh bond cleavage/reformation catalyzed by water to form *rac*-**2a**$^{2-}$·$(Na^+)_2$. The transformations between *rac*-**2a**$^{2-}$·$(Na^+)_2$ and *meso*-**2b**$^{2-}$·$(Na^+)_2$ were also possible in a controllable manner in the presence of a catalytic amount of *p*-TsOH with an appropriate amount of water at 35 °C (Figure 5).

In anhydrous CD_3CN, however, the *meso*-**2b**$^{2-}$·$(Na^+)_2$ was further converted to another helicate while maintaining its *meso*-framework, namely *meso*-**2c**$^{2-}$·$(Na^+)_2$, through dehydration upon heating because the Ti-OPh bond cleavage reaction of *meso*-**2b**$^{2-}$·$(Na^+)_2$ is suppressed in the absence of water even at high temperature, thus selectively producing the moisture sensitive *meso*-**2c**$^{2-}$·$(Na^+)_2$ instead of *rac*-**2a**$^{2-}$·$(Na^+)_2$. This *meso*-**2b**$^{2-}$-to-*meso*-**2c**$^{2-}$ transformation was significantly promoted in the presence of cryptand [2.2.1], which contributes to removing Na^+ ions coordinating to the *meso*-**2b**$^{2-}$, leading to the formation of the highly-active *meso*-**2b**$^{2-}$·$(Na^+\subset[2.2.1])_2$ species toward dehydration at high temperature. This speculation was supported by the fact that the *meso*-**2b**$^{2-}$·$(TBA^+)_2$-to-*meso*-**2c**$^{2-}$·$(TBA^+)_2$ transformation proceeded through dehydration in the absence of cryptand [2.2.1] (Figure S13). Upon cooling, the backward *meso*-**2c**$^{2-}$-to-*meso*-**2b**$^{2-}$ transformation readily proceeds via hydration, thus this reversible transformation between *meso*-**2b**$^{2-}$ and *meso*-**2c**$^{2-}$ can be controlled by temperature resulting from thermoresponsive dehydration/hydration.

Although the reversible transformations between *rac*-**2a**$^{2-}$ and *meso*-**2b**$^{2-}$ and between *meso*-**2b**$^{2-}$·$(Na^+)_2$ and *meso*-**2c**$^{2-}$·$(Na^+)_2$ take place via direct pathways, the transformation (isomerization) between the structural isomers of *rac*-**2a**$^{2-}$ and *meso*-**2c**$^{2-}$ proceeds in a stepwise manner through the formation of the *meso*-**2b**$^{2-}$ intermediate. This is because (1) a moderate amount of water with or without a catalytic amount of an acid is indispensable for the transformation between the *rac*-**2a**$^{2-}$ and *meso*-**2b**$^{2-}$ helicates in order to cleave at least one of the eight Ti–OPh bonds at the two Ti(IV) centers, followed by reforming of the *rac*-**2a**$^{2-}$ and *meso*-**2b**$^{2-}$ helicate, and (2) the moisture-sensitive *meso*-**2c**$^{2-}$ readily undergoes hydration to form the *meso*-**2b**$^{2-}$ in the presence of a moderate amount of water.

CONCLUSION

In summary, we have demonstrated a unique three-state molecular control based on the reversible transformations between the three discrete double-stranded dinuclear Ti(IV) helicates possessing a mono-μ-oxo (*rac*-**2a**$^{2-}$ and *meso*-**2c**$^{2-}$) or a bis(μ-hydroxo) (*meso*-**2b**$^{2-}$) bridging ligand that can be regulated by changing the water content coupled with temperature. The single-crystal X-ray and DFT calculated structures of the helicates together with the 1D and 2D NMR and CSI mass measurement results revealed the structural and mechanistic details of the reversible transformations between the three different helicates. We found that water molecules play key roles as a reactant, product, and catalyst during the hydration, dehydration, and dynamic cleavage/reformation of the Ti-OPh bonds, respectively. A large amount of water promotes the hydration accompanied by the reversible Ti-OPh bond cleavage/reformation upon heating, thereby inducing the transformation of the mono-μ-oxo-bridged *racemo*-helicate (*rac*-**2a**$^{2-}$) into the bis(μ-hydroxo)-bridged *meso*-helicate (*meso*-**2b**$^{2-}$), whereas the reverse transformation proceeds by reducing the water content to a moderate level at a high temperature. This reversible *meso*-**2b**$^{2-}$-to-*racemo*-**2a**$^{2-}$ transformation can be controlled over switching off by removal of the water because the cleavage of the Ti-OPh bonds is completely prevented in the absence of water, thus dehydration of the bis(μ-hydroxo) bridged *meso*-**2b**$^{2-}$ preferentially proceeds to form the mono-μ-oxo bridged *meso*-helicate (*meso*-**2c**$^{2-}$) while maintaining the *meso*-framework upon heating. A further reversible transformation readily takes place upon cooling. The reversible transformations between the *rac*-**2a**$^{2-}$ and *meso*-**2b**$^{2-}$ helicates are also promoted in the presence of a catalytic amount of an acid with an appropriate amount of water, which remarkably accelerates the reactions at lower temperature.

These findings may provide not only a mechanistic insight into a water-mediated and/or an acid-catalyzed transformation of dinuclear metal complexes possessing bridging ligands but also a means for the rational design of supramolecular multinuclear metal catalysts whose catalytic activity and substrate selectivity would be controlled by the water-mediated and/or acid-catalyzed transformation. However, there is no precedent for asymmetric or catalytic reactions with dinuclear Ti(IV)-based helicates as a catalyst in the literature. This is probably because almost all Ti(IV)-based helicates prepared so far have a saturated six-coordination Ti(IV) geometry. Therefore, their catalytic activities will not be expected. Among three helicates, the *rac*-**2a**$^{2-}$·$(Na^+)_2$ has a five-coordinate Ti(IV) geometry with a site of unsaturation. Therefore, its enantioselective catalytic activity will be expected[72] after complete separation of *racemic rac*-**2a**$^{2-}$·$(Na^+)_2$ into optically pure enantiomers. Work to this goal is now in progress in our group.

ASSOCIATED CONTENT

Supporting Information

The Supporting Information is available free of charge on the ACS Publications website at DOI: xxxx.
Full experimental details and additional spectroscopic data (PDF)

AUTHOR INFORMATION

Corresponding Author

*yashima@chembio.nagoya-u.ac.jp

ORCID

Naoki Ousaka: 0000-0002-3398-3328
Daisuke Taura: 0000-0002-5396-5573
Eiji Yashima: 0000-0001-6307-198X

Present Address

§ Present Address: Molecular Engineering Institute, Kyushu Institute of Technology, Tobata-ku, Kitakyushu, 804-8550, Japan.

Notes

The authors declare no competing financial interest.

ACKNOWLEDGMENT

We thank Dr. Hiroki Iida (Shimane University) for X-ray crystallographic analysis of *rac*-**2a**$^{2-}$·((*S*)-**3**$^+$)$_2$ and *meso*-**2b**$^{2-}$·$(Na^+)_2$. We are deeply grateful to Professor Makoto Yamashita and Mr. Satoshi Kurumada (Nagoya University) for their invaluable assistance in the single crystal formation of *meso*-**2c**$^{2-}$·$(Na^+\subset[2.2.1])_2$ and *meso*-**2c**$^{2-}$·$(TBA^+)_2$ and X-ray diffraction measurements. This work was supported in part by JSPS KAKENHI (Grant-in-Aid for Specially Promoted Research, no. 18H05209 (E.Y. and T.I.) and Grant-in-Aid for Young Scientists (B), no. 17K14470 (N.O.)).

REFERENCES

(1) Caulder, D. L.; Raymond, K. N. Supermolecules by Design. *Acc. Chem. Res.* **1999**, *32*, 975-982.

(2) Fujita, M.; Tominaga, M.; Hori, A.; Therrien, B. Coordination Assemblies from a Pd(II)-Cornered Square Complex. *Acc. Chem. Res.* **2005**, *38*, 369-378.

(3) Saalfrank, R. W.; Maid, H.; Scheurer, A. Supramolecular Coordination Chemistry: The Synergistic Effect of Serendipity and Rational Design. *Angew. Chem., Int. Ed.* **2008**, *47*, 8794-8824.

(4) Ward, M. D. Polynuclear Coordination Cages. *Chem. Commun.* **2009**, 4487-4499.

(5) Jin, P.; Dalgarno, S. J.; Atwood, J. L. Mixed Metal-Organic Nanocapsules. *Coord. Chem. Rev.* **2010**, *254*, 1760-1768.

(6) Chakrabarty, R.; Mukherjee, P. S.; Stang, P. J. Supramolecular Coordination: Self-Assembly of Finite Two- and Three-Dimensional Ensembles. *Chem. Rev.* **2011**, *111*, 6810-6918.

(7) Cook, T. R.; Stang, P. J. Recent Developments in the Preparation and Chemistry of Metallacycles and Metallacages via Coordination. *Chem. Rev.* **2015**, *115*, 7001-7045.

(8) Zarra, S.; Wood, D. M.; Roberts, D. A.; Nitschke, J. R. Molecular Containers in Complex Chemical Systems. *Chem. Soc. Rev.* **2015**, *44*, 419-432.

(9) Zhang, D.; Ronson, T. K.; Nitschke, J. R. Functional Capsules via Subcomponent Self-Assembly. *Acc. Chem. Res.* **2018**, *51*, 2423-2436.

(10) Leininger, S.; Olenyuk, B.; Stang, P. J. Self-Assembly of Discrete Cyclic Nanostructures Mediated by Transition Metals. *Chem. Rev.* **2000**, *100*, 853-908.

(11) Oliveri, C. G.; Ulmann, P. A.; Wiester, M. J.; Mirkin, C. A. Heteroligated Supramolecular Coordination Complexes Formed via the Halide-Induced Ligand Rearrangement Reaction. *Acc. Chem. Res.* **2008**, *41*, 1618-1629.

(12) Lehn, J.-M.; Rigault, A.; Siegel, J.; Harrowfield, J.; Chevrier, B.; Moras, D. Spontaneous Assembly of Double-Stranded Helicates from Oligobipyridine Ligands and Copper(I) Cations: Structure of an Inorganic Double Helix. *Proc. Natl. Acad. Sci. USA* **1987**, *84*, 2565-2569.

(13) Constable, E. C. Oligopyridines as Helicating Ligands. *Tetrahedron* **1992**, *48*, 10013-10059.

(14) Lehn, J.-M. *Supramolecular Chemistry: Concepts and Perspectives*. VCH: Weinheim, 1995; Chapter 9.

(15) Piguet, C.: Bernardinelli, G.; Hopfgartner, G. Helicates as Versatile Supramolecular Complexes. *Chem. Rev.* **1997**, *97*, 2005-2062.

(16) Albrecht, M. Dicatechol Ligands: Novel Building-Blocks for Metallo-Supramolecular Chemistry. *Chem. Soc. Rev.* **1998**, *27*, 281-288.

(17) Albrecht, M. "Let's Twist Again" Double-Stranded, Triple-Stranded, and Circular Helicates. *Chem. Rev.* **2001**, *101*, 3457-3498.

(18) Howson, S. E.; Scott, P. Approaches to the Synthesis of Optically Pure Helicates. *Dalton Trans.* **2011**, *40*, 10268-10277.

(19) Ousaka, N.; Takeyama, Y.; Yashima, E. Dinuclear Metal Complexes Composed of Peptide Chains: Solvent-Induced Switching and Inversion of the Metal-Centered Chirality. *Chem. Sci.* **2012**, *3*, 466-469.

(20) Akine, S.; Sairenji, S.; Taniguchi, T.; Nabeshima, T. Stepwise Helicity Inversions by Multisequential Metal Exchange. *J. Am. Chem. Soc.* **2013**, *135*, 12948-12951.

(21) Chen, X.; Gerger, T. M.: Räuber, C.; Raabe, G.; Göb, C.; Oppel, I. M.; Albrecht, M. A Helicate-Based Three-State Molecular Switch. *Angew. Chem., Int. Ed.* **2018**, *57*, 11817-11820.

(22) Wang, W.; Wang, Y.-X.; Yang, H.-B. Supramolecular Transformations within Discrete Coordination-Driven Supramolecular Architectures. *Chem. Soc. Rev.* **2016**, *45*, 2656-2693.

(23) Jung, O.-S.; Kim, Y. J.; Lee, Y.-A.; Park, J. K.; Chae, H. K. Smart Molecular Helical Springs as Tunable Receptors. *J. Am. Chem. Soc.* **2000**, *122*, 9921-9925.

(24) Nabeshima, T.; Yoshihira, Y.; Saiki, T.; Akine, S.; Horn, E. Remarkably Large Positive and Negative Allosteric Effects on Ion Recognition by the Formation of a Novel Helical Pseudocryptand. *J. Am. Chem. Soc.* **2003**, *125*, 28-29.

(25) Berni, E.; Kauffmann, B.; Bao, C.; Lefeuvre, J.; Bassani, D. M.; Huc, I. Assessing the Mechanical Properties of a Molecular Spring. *Chem. Eur. J.* **2007**, *13*, 8463-8469.

(26) Kim, H.-J.; Lee, E.; Park, H.-s.; Lee, M. Dynamic Extension−Contraction Motion in Supramolecular Springs. *J. Am. Chem. Soc.* **2007**, *129*, 10994-10995.

(27) Ferrand, Y.; Kendhale, A. M.; Garric, J.; Kauffmann, B.; Huc, I. Parallel and Antiparallel Triple Helices of Naphthyridine Oligoamides. *Angew. Chem., Int. Ed.* **2010**, *49*, 1778-1781.

(28) Hashimoto, T.; Nishimura, T.; Lim, J. M.; Kim, D.; Maeda, H. Formation of Metal-Assisted Stable Double Helices in Dimers of Cyclic Bis-Tetrapyrroles That Exhibit Spring-Like Motion. *Chem. Eur. J.* **2010**, *16*, 11653-11661.

(29) Miwa, K.; Furusho, Y.; Yashima, E. Ion-Triggered Spring-Like Motion of a Double Helicate Accompanied by Anisotropic Twisting. *Nat. Chem.* **2010**, *2*, 444-449.

(30) Yamamoto, S.; Iida, H.; Yashima, E. Guest-Induced Unidirectional Dual Rotary and Twisting Motions of a Spiroborate-Based Double-Stranded Helicate Containing a Bisporphyrin Unit. *Angew. Chem., Int. Ed.* **2013**, *52*, 6849-6853.

(31) Suzuki, Y.; Nakamura, T.; Iida, H.; Ousaka, N.; Yashima, E. Allosteric Regulation of Unidirectional Spring-Like Motion of Double-Stranded Helicates. *J. Am. Chem. Soc.* **2016**, *138*, 4852-4859.

(32) Ousaka, N.; Shimizu, K.; Suzuki, Y.; Iwata, T.; Itakura, M.; Taura, D.; Iida, H.; Furusho, Y.; Mori, T.; Yashima, E. Spiroborate-Based Double-Stranded Helicates: Meso-to-Racemo Isomerization and Ion-Triggered Springlike Motion of the Racemo-Helicate. *J. Am. Chem. Soc.* **2018**, *140*, 17027-17039.

(33) Ousaka, N.; Yamamoto, S.; Iida, H.; Iwata, T.; Ito, S.; Hijikata, Y.; Irle, S.; Yashima, E. Water-Mediated Deracemization of a Bisporphyrin Helicate Assisted by Diastereoselective Encapsulation of Chiral Guests. *Nat. Commun.* **2019**, *10*, 1457.

(34) Berl, V.; Huc, I.; Khoury, R. G.; Krische, M. J.; Lehn, J.-M. Interconversion of Single and Double Helices Formed from Synthetic Molecular Strands. *Nature* **2000**, *407*, 720-723.

(35) Huc, I. Aromatic Oligoamide Foldamers. *Eur. J. Org. Chem.* **2004**, *2004*, 17-29.

(36) Ferrand, Y.; Huc, I. Designing Helical Molecular Capsules Based on Folded Aromatic Amide Oligomers. *Acc. Chem. Res.* **2018**, *51*, 970-977.

(37) Yashima, E.; Ousaka, N.; Taura, D.; Shimomura, K.; Ikai, T.; Maeda, K. Supramolecular Helical Systems: Helical Assemblies of Small Molecules, Foldamers, and Polymers with Chiral Amplification and Their Functions. *Chem. Rev.* **2016**, *116*, 13752-13990.

(38) Raynal, M.; Ballester, P.; Vidal-Ferran, A.; van Leeuwen, P. W. N. M. Supramolecular Catalysis. Part 1: Non-Covalent Interactions as a Tool for Building and Modifying Homogeneous Catalysts. *Chem. Soc. Rev.* **2014**, *43*, 1660-1733.

(39) Yeung, C.-T.; Yeung, H.-L.; Tsang, C.-S.; Wong, W.-Y.; Kwong, H.-L. Supramolecular Double Helical Cu(I) Complexes for Asymmetric Cyclopropanation. *Chem. Commun.* **2007**, 5203-5205.

(40) Sham, K.-C.; Yeung, H.-L.; Yiu, S.-M.; Lau, T.-C.; Kwong, H.-L. New Binuclear Double-Stranded Manganese Helicates as Catalysts for Alkene Epoxidation. *Dalton Trans.* **2010**, *39*, 9469-9471.

(41) Chinnaraja, E.; Arunachalam, R.; Suresh, E.; Sen, S. K.; Natarajan, R.; Subramanian, P. S. Binuclear Double-Stranded Helicates and Their Catalytic Applications in Desymmetrization of Mesodiols. *Inorg. Chem.* **2019**, *58*, 4465-4479.

(42) Albrecht, M.; Kotila, S. Formation of a "Meso-Helicate" by Self-Assembly of Three Bis(catecholate) Ligands and Two Titanium(Iv) Ions. *Angew. Chem. Int. Ed. Engl.* **1995**, *34*, 2134-2137.

(43) Enemark, E. J.; Stack, T. D. P. Synthesis and Structural Characterization of a Stereospecific Dinuclear Gallium Triple Helix: Use of the *trans*-Influence in Metal-Assisted Self-Assembly. *Angew. Chem. Int. Ed. Engl.* **1995**, *34*, 996-998.

(44) Albrecht, M.; Kotila, S. Stabilization of an Unusual Coordination Geometry at Li^+ in the Interior of a Cryptand-Type Helicate. *Angew. Chem. Int. Ed. Engl.* **1996**, *35*, 1208-1210.

(45) Enemark, E. J.; Stack, T. D. P. Spectral and Structural Characterization of Two Ferric Coordination Modes of a Simple Bis(catecholamide) Ligand: Metal-Assisted Self-Assembly in a Siderophore Analog. *Inorg. Chem.* **1996**, *35*, 2719-2720.

(46) Kersting, B.; Meyer, M.; Powers, R. E.; Raymond, K. N. Dinuclear Catecholate Helicates: Their Inversion Mechanism. *J. Am. Chem. Soc.* **1996**, *118*, 7221-7222.

(47) Albrecht, M.; Schneider, M.; Röttele, H. Template-Directed Self-Recognition of Alkyl-Bridged Bis(catechol) Ligands in the Formation of Helicate-Type Complexes. *Angew. Chem., Int. Ed.* **1999**, *38*, 557-559.

(48) Albrecht, M.; Napp, M.; Schneider, M.; Weis, P.; Fröhlich, R. Dinuclear Titanium(IV) Complexes from Amino Acid Bridged Dicatechol Ligands: Formation, Structure, and Conformational Analysis. *Chem. Eur. J.* **2001**, *7*, 3966-3975.

(49) Albrecht, M.; Napp, M.; Schneider, M.; Weis, P.; Fröhlich, R. Kinetic Thermodynamic Control of the Self-Assembly of Isomeric Double-Stranded Dinuclear Titanium(IV) Complexes from a Phenylalanine-Bridged Dicatechol Ligand. *Chem. Commun.* **2001**, 409-410.

(50) Kiehne, U.; Lützen, A. Synthesis of Bis(catechol) Ligands Derived from Tröger's Base and Their Dinuclear Triple-Stranded Complexes with Titanium(IV) Ions. *Eur. J. Org. Chem.* **2007**, *2007*, 5703-5711.

(51) Haino, T.; Shio, H.; Takano, R.; Fukazawa, Y. Asymmetric Induction of Supramolecular Helicity in Calix[4]arene-Based Triple-Stranded Helicate. *Chem. Commun.* **2009**, 2481-2483.

(52) Diebold, C.; Mobian, P.; Huguenard, C.; Allouche, L.; Henry, M. Spontaneous Symmetry Breaking During Self-Assembly of a Double Stranded Biphenolate-Based Ti(IV)-Helicate. *Inorg. Chem.* **2010**, *49*, 6369-6371.

(53) Weekes, D. M.; Diebold, C.; Mobian, P.; Huguenard, C.; Allouche, L.; Henry, M. A Remarkable Solvent Effect on the Nuclearity of Neutral Titanium(IV)-Based Helicate Assemblies. *Chem. Eur. J.* **2014**, *20*, 5092-5101.

(54) Macker, E.; Barloy, L.; Chaumont, A.; Kyritsakas, N.; Vincent, B.; Henry, M.; Mobian, P. Evaluation of the Stereoselectivity for Titanium(IV)-Based Coordination Entities Induced by the Enantiopure Diphenylethene-1,2-Diamine Ligand. *Inorg. Chim. Acta* **2019**, *498*, 119119.

(55) Rao, M. L. N.; Houjou, H.; Hiratani, K. Self-Assembly of Double Stranded Dinuclear Titanium(IV)–Schiff Base Complexes and Formation of Intramolecular μ-Oxo Bridges. *Chem. Commun.* **2002**, 420-421.

(56) Bernardinelli, G.; Seidel, T. M.; Kündig, E. P.; Prins, L. J.; Kolarovic, A.; Mba, M.; Pontini, M.; Licini, G. Stereoselective Dimerization of Racemic C_3-Symmetric Ti(IV) Amine Triphenolate Complexes. *Dalton Trans.* **2007**, 1573-1576.

(57) Kreickmann, T.; Diedrich, C.; Pape, T.; Huynh, H. V.; Grimme, S.; Hahn, F. E. Metallosupramolecular Chemistry with Bis(benzene-*o*-dithiolato) Ligands. *J. Am. Chem. Soc.* **2006**, *128*, 11808-11819.

(58) Albrecht, M.; Mirtschin, S.; de Groot, M.; Janser, I.; Runsink, J.; Raabe, G.; Kogej, M.; Schalley, C. A.; Fröhlich, R. Hierarchical Assembly of Helicate-Type Dinuclear Titanium(IV) Complexes. *J. Am. Chem. Soc.* **2005**, *127*, 10371-10387.

(59) Albrecht, M.; Isaak, E.; Baumert, M.; Gossen, V.; Raabe, G.; Fröhlich, R. "Induced Fit" in Chiral Recognition: Epimerization upon Dimerization in the Hierarchical Self-Assembly of Helicate-Type Titanium(IV) Complexes. *Angew. Chem., Int. Ed.* **2011**, *50*, 2850-2853.

(60) Albrecht, M. Synthesis of a Chiral Alkyl-Bridged Bis(catecholamide) Ligand for the Self-Assembly of Enantiomerically Pure Helicates. *Synlett* **1996**, *6*, 565-567.

(61) Albrecht, M.; Janser, I.; Fleischhauer, J.; Wang, Y.; Raabe, G.; Fröhlich, R. An Enantiomerically Pure Dinuclear Triple-Stranded Helicate: X-Ray Structure, CD Spectroscopy and DFT Calculations. *Mendeleev Commun*. **2004**, *14*, 250-253.

(62) Veljković, D. Ž.; Janjić, G. V.; Zarić, S. D. Are C–H···O Interactions Linear? The Case of Aromatic CH Donors. *CrystEngComm* **2011**, *13*, 5005-5010.

(63) We did not optimize this reaction condition with respect to the amount of water.

(64) Furusho, Y.; Miwa, K.; Asai, R.; Yashima, E. Synthesis and Helical Structure of Spiroborate-Based Double-Stranded Helicate with Oligophenol Strands Bearing Bipyridine Units. *Chem. Eur. J.* **2011**, *17*, 13954-13957.

(65) Taura, D.; Min, H.; Katan, C.; Yashima, E. Synthesis of a Double-Stranded Spiroborate Helicate Bearing Stilbene Units and Its Photoresponsive Behaviour. *New J. Chem.* **2015**, *39*, 3259-3269.

(66) Taura, D.; Shimizu, K.; Yokota, C.; Ikeda, R.; Suzuki, Y.; Iida, H.; Ousaka, N.; Yashima, E. Fluorescent Molecular Spring That Visualizes the Extension and Contraction Motions of a Double-Stranded Helicate Bearing Terminal Pyrene Units Triggered by Release and Binding of Alkali Metal Ions. *Chem. Commun.* **2019**, *55*, 12084-12087.

(67) Ito, M.; Ikai, T.; Yamamoto, S.; Taura, D.; Ousaka, N.; Yashima, E. Chiral Guest-Induced Catalytic Deracemization of a Spiroborate-Based Double-Stranded Helicate Bearing a Bisporphyrin Unit with Acids. *Chem. Lett.* **2020**, *49,* 1030-1033.

(68) The differences in the molar ratios of *meso*-**2b**$^{2-}$ and *meso*-**2c**$^{2-}$ formed at an equilibrium at 75 °C (Figures 6d and S11b) may be due to a highly moisture-sensitivity of *meso*-**2c**$^{2-}$.

(69) This *meso*-**2c**$^{2-}\cdot(TBA^+)_2$ helicate was synthesized from the corresponding *meso*-**2b**$^{2-}\cdot(TBA^+)_2$ through dehydration upon heating at 75 °C, which proceeded in the absence of cryptand [2.2.1] (Figure S13). For the synthesis of *meso*-**2b**$^{2-}\cdot(TBA^+)_2$ and *meso*-**2c**$^{2-}\cdot(TBA^+)_2$ and the CSI mass spectrum of the *meso*-**2c**$^{2-}\cdot(TBA^+)_2$, see SI and Figure S17, respectively.

(70) As anticipated, the ^{1}H and ^{13}C NMR spectra of the *meso*-**2b**$^{2-}\cdot(Na^+\subset[2.2.1])_2$ and *meso*-**2b**$^{2-}\cdot(TBA^+)_2$ helicates as well as those of the *meso*-**2c**$^{2-}\cdot(Na^+\subset[2.2.1])_2$ and *meso*-**2c**$^{2-}\cdot(TBA^+)_2$ helicates are very similar to each other (Figures S4 and S5). For the *meso*-**2b**$^{2-}\cdot(TBA^+)_2$-to-*meso*-**2c**$^{2-}\cdot(TBA^+)_2$ transformation, see Figure S13.

(71) Wannere, C. S.; Schleyer, P. v. R. How Do Ring Currents Affect ^{1}H NMR Chemical Shifts? *Org. Lett.* **2003**, *5*, 605-608.

(72) Belokon', Y. N.; Green, B; Ikonnikov, N. S.; Larichev, V. S.; Lokshin, B. V.; Moscalenko, M; A.; North, M.; Orizu, C.; Peregudov, A. S.; Timofeeva, G. I. Mechanistic Investigation of the Asymmetric Addition of Trimethylsilyl Cyanide to Aldehydes Catalysed by Dinuclear Chiral (Salen)titanium Complexes. *Eur. J. Org. Chem.* **2000**, 2655-2661.

Table of Contents Artwork

Water-Mediated Reversible Control of Three-State Helicates